A fast stroboscopic spectral method for rotating systems in numerical relativity

Silvano Bonazzola, José-Luis Jaramillo, Jerome Novak

A fast stroboscopic spectral method for rotating systems in numerical relativity

Silvano Bonazzola[1]‡, **José Luis Jaramillo**[2]§ **and Jérôme Novak**[1]‖

[1] Laboratoire Univers et Théories, UMR 8102 du C.N.R.S., Observatoire de Paris, F-92195 Meudon Cedex, France
[2] Instituto de Astrofísica de Andalucía, CSIC, Apartado Postal 3004, Granada 18080, Spain

Abstract. We present a numerical technique for solving evolution equations, as the wave equation, in the description of rotating astrophysical compact objects in comoving coordinates, which avoids the problems associated with the light cylinder. The technique implements a fast spectral matching between two domains in relative rotation: an inner spherical domain, comoving with the sources and lying strictly inside the light cylinder, and an outer inertial spherical shell. Even though the emphasis is placed on spectral techniques, the matching is independent of the specific manner in which equations are solved inside each domain, and can be adapted to different schemes. We illustrate the strategy with some simple but representative examples.

PACS numbers: 04.25.Dm, 04.30.Db, 02.70.Hm

‡ Email address: Silvano.Bonazzola@obspm.fr
§ Email address: jarama@iaa.es
‖ Email address: Jerome.Novak@obspm.fr

1. Introduction

A general motivation for undertaking this project is suggested by the numerical study of astrophysical compact objects, e.g. neutron stars and black holes, individually rotating or in bound binary systems, where the dynamics of the interaction field is described by a system of equations which is (at least, in part) hyperbolic. An example of this is provided by Einstein equations in General Relativity or the Maxwell equations in modeling the pulsar magnetosphere. The main objective of this paper is to present a general numerical technique for solving the dynamics of such systems, with the example of the scalar wave equation as the equation governing the evolution of the system.

The study of the general motion of compact finite bodies, say black holes (BH) or neutron stars (NS) for concreteness, in a fixed numerical grid represents a serious challenge from a numerical point of view. Examples of this Eulerian approach to the motion problem can be found in Refs. [1, 2]. Recent examples of moving BH in the context of binary systems have been successfully developed an implemented both using excision techniques [3, 4, 5] and moving punctures [6, 7, 8]. However, we would find unfortunate if these extraordinary achievements actually shadowed the development of parallel approaches which employ independent analytical formulations and/or numerical methods. This is the case of constrained evolution formalisms (e.g. see Ref. [9]) and of the use of spectral methods (already initiated in the binary BH case in Ref. [10]). More concretely, the use of spectral methods seem to favor an excision approach for BH evolution where the coordinate location of the excised surface do not change significantly in time [10]. On the other hand constrained evolutions schemes, in combination with a comoving coordinate systems, can be employed to endow the excised surface with a geometrical character by enforcing appropriate inner boundary conditions in some of the elliptic (constraint) equations, something that can be relevant both for the numerical stability of the code and the study of some quasi-local geometrical properties of BH space-times [11]. These elements indicate the interest in pursuing the study of corotating coordinate systems.

Regarding the presence of matter, namely the NS case, experience in our group shows the convenience of using a Lagrangian scheme to describe the surface of the NS and a Eulerian one for the interior. Details of this technique can be found in Refs. [12] and in [13] where a steady state approximation was used. Building accurate non-stationary numerical models of magnetized rotating neutron stars and of the surrounding magnetosphere might thus also be easier with such codes, able to naturally follow the surface of the star. Therefore, an interesting alternative strategy to the Eulerian approach consists in reducing the motion of the body in the grid by choosing a comoving coordinate system. However, the use of a single rotating coordinate system faces the problems coming from the superluminal motion of the grid at distances to the rotation center larger than the light cylinder radius (see next section for the definition of the latter). Part of these problems, related to the tensorial nature of the rotating fields, can be handled by using appropriate techniques (e.g. the "dual-coordinate frames" introduced in Ref. [10]).

The aim of this paper is to propose a complementary approach that bypasses the light cylinder issue in the case of a scalar field wave equation, using an intermediate strategy in which space is split into two domains: first, an internal spherical one of radius R_* containing the sources and set inside the light cylinder, and then an external domain with inner boundary given by the sphere $r = R_*$ and whose outer

radius is larger than the considered wavelength in order to impose approximate (or exact) outgoing wave conditions. The exterior domain is described in terms of non-rotating coordinates and simultaneously, a rigidly¶ rotating coordinate system is set in the interior domain whose angular velocity is fixed by a physical scale in the problem (e.g. the orbital frequency in a binary problem). Each domain could be further decomposed into smaller ones, but this paper focuses on the matching conditions and not in the specific manner in which the equations are solved inside each domain. The main problem we address here is then the matching technique between domains in relative rotation in a multi-domain spectral scheme. In particular, if we consider the spherical boundary between the inner and outer domains, and denote by N_θ and N_φ the number of sampling points in the θ and φ spherical-coordinate directions, then the technique for matching the solutions at this intermediate boundary is said to be fast in the following sense. The most straightforward approach is just to write the matching system, using a spectral summation, at every point of each grid, which requires $N_\theta^2 N_\phi^2$ operations. Our approach here can be performed with only $N_\theta \cdot N_\varphi$ instead, with a so-called *stroboscopic* technique based on spectral methods.

The paper is organized as follows: Section 2 describes the simple model we want to study and specifies the light cylinder problem, Section 3 gives the numerical details of our matching technique and some outlines of the implementation, Section 4 shows the results of two test-problems, and finally Section 5 contains concluding remarks. We emphasize that in this work we address the description of a technique enabling us to study the dynamics of a system with a rotating source. Even though the main problem we have in mind is the study of the evolution problem for some given initial data, we can also employ these resolution techniques in order to construct the initial data themselves by assuming additional hypotheses and/or approximations for some given terms in the equations. In particular, in the description of the present technique we do not make any assumption about the existence of approximate Killing vectors, something that would have to be incorporated in the equations themselves in the construction of initial data of binaries in quasi-circular motion (see Refs. [15, 16, 17]) for different approaches, and below).

2. Light cylinder and simplified mathematical models

The resolution of the full Einstein Equations (EE) can be reduced to solve a couple of wave equations for two independent scalar potentials if one uses a constrained scheme, where the ten EE have been decomposed as four elliptic constraint equations, four gauge degrees of freedom and two scalar wave-like evolution equations [9]. In this section we consider the linearized version of the actual problem for one of the potentials. This is quite general since in the overall problem for the solution of the EE, we shall perform exactly the same matching for every wave-like equation.

In particular, consider a non-rotating coordinate system (t, r, θ, φ) and a field Φ satisfying

$$\left(\frac{1}{c^2}\partial_t^2 - \Delta\right)\Phi = n, \tag{1}$$

where c is the propagation speed of the field and n denotes the matter mass density (renormalized with a $4\pi G$ factor). We assume that matter is contained in a compact

¶ The notion of "rigidity" employed here, is defined in terms of a fiducial time-independent flat 3-metric f_{ij}, as introduced in the constrained evolution formalism presented in Ref. [9].

region bounded by characteristic radius R_*. Defining a spherical coordinate system rotating rigidly with constant angular velocity Ω, $(t' = t, r' = r, \theta' = \theta, \varphi' = \varphi + \Omega\, t)$, and writing explicitly the Laplacian, the wave equation becomes

$$\left[\frac{1}{c^2}\partial^2_{t'} + 2\frac{\Omega}{c^2}\partial_{t'}\partial_{\varphi'} - \partial^2_{r'} - \frac{2}{r'}\partial_{r'} \right. \tag{2}$$
$$\left. -\frac{1}{r'^2}\left(\partial^2_{\theta'} + \frac{\cos\theta'}{\sin\theta'}\partial_{\theta'} + \frac{1}{\sin^2\theta'}\left(1 - \left(\frac{\Omega r' \sin\theta'}{c}\right)^2\right)\partial^2_{\varphi'}\right)\right]\Phi = n$$

We note that in our formulation of the problem, there appears a second characteristic scale, given by the vanishing of the factor $\left(1 - \left(\frac{\Omega r \sin\theta'}{c}\right)^2\right)$. This defines the *light cylinder* of radius $R_L = \frac{c}{\Omega}$, with respect to the rotation axis, where the vector $\partial_{t'}$ (corresponding to $\partial_t - \Omega\partial_\varphi$ in the inertial system) becomes null. The total operator in Eq. (2) is hyperbolic everywhere. However we note that, even though the spatial part of the operator is negative definite in the region inside the light cylinder, $r < R_L$, this feature is lost for $r > R_L$. Motivated by this remark (see discussion below), we will always assume the hypothesis that $R_* < R_L$. This assumption will be eventually justified on physical grounds.

As mentioned above, in the present work we study the dynamical evolution of a system with a given matter source $n(t, r, \theta, \varphi)$. Then, our strategy to describe the dynamics consists in solving the equations in different coordinate systems depending on the domain. In concrete terms: a) we choose rotating coordinates in the domain containing matter, i.e. we solve Eq. (2) for $r \leq R_*$, and b) we employ an inertial coordinate system in the exterior region, i.e for $r \geq R_*$ we solve Eq. (1).

Even though we are focused on the general evolution problem, it is convenient to highlight that the existence of the light cylinder is an important issue in the construction of quasi-stationary rotating configurations of binary systems. The introduction of a helical Killing vector has been used in the literature (cf. [15, 16, 17]) in order to model slow-motion adiabatic configurations of binary NS and BH systems. In particular, regarding Eq. (2) this imposition of the vector $\partial_{t'}$ as a helical symmetry of the solution, implies the vanishing of the first two terms in the left-hand-side of the equation. A discussion of the numerical technical issues of the resulting mixed-type partial differential equation, that is elliptic inside the light cylinder and hyperbolic outside, can be found in the series of works on quasi-stationary binary inspiral [18, 19, 20, 21], as well as the so-called "periodic standing-wave" approximation [22, 23, 24, 25]. See also Ref. [26] for a study of its mathematical well-posedness. In this context of potential numerical problems associated with the type of the spatial part of the differential operator, the advantage of our approach is that the light cylinder problem is completely avoided, since $R_* < R_L$. Indeed, in the interior domain the differential operator presents a standard "negative" spatial part and there are no problems in solving numerically Eq. (2), whereas no light cylinder problem shows up in Eq. (1) in the exterior domain.

We conclude the section by emphasizing that with this point of view, the light cylinder problem is replaced by a matching problem, which is much easier to treat numerically. We therefore state the main problem to be addressed in this approach, and which defines the goal of the paper: the implementation of the matching between the solutions in both domains. Next section presents a fast$^+$ matching numerical

$^+$ By fast we mean that the number of operations is not larger than $N \cdot \log N$ for each dimension,

algorithm.

3. Numerical strategy

We introduce the following dimensionless variables ξ and τ in the inner and outer domains:

$$\begin{aligned} \xi' &= \frac{r'}{R_*}, \quad \tau' = \frac{t'}{P} \quad (\text{for } r' \leq R_*), \quad \text{and} \\ \xi &= \frac{r}{R_*}, \quad \tau = \frac{t}{P} \quad (\text{for } r \geq R_*), \end{aligned} \tag{3}$$

where $P = 2\pi/\Omega$ is the rotation period. Making use of these coordinates and denoting the field Φ by $\Phi^<$ in the interior domain ($0 \leq \xi \leq 1$), and by $\Phi^>$ in the exterior domain ($\xi \geq 1$), we write Eqs. (1) and (2) in the following dimensionless form

$$\left(\frac{\partial^2}{\partial\tau^2} - C^2\bar{\Delta}\right)\Phi^> = 0 \quad , \tag{4}$$

$$\left[\frac{\partial^2}{\partial\tau'^2} + 2(2\pi)\frac{\partial^2}{\partial\tau'\partial\phi'} + (2\pi)^2\frac{\partial^2}{\partial\phi'^2} - C^2\bar{\Delta}\right]\Phi^< = \bar{n} \tag{5}$$

where

$$C = 2\pi\frac{R_L}{R_*}, \tag{6}$$

is the dimensionless "light velocity", $\bar{\Delta}$ is the Laplacian in terms of the dimensionless radial coordinate ξ, and $\bar{n} = R_*^2C^2 \cdot n$ is the dimensionless matter density (note that the dimensionless angular velocity is 2π).
In order to simplify the presentation, and since the notation should be self-explanatory in the following, we shall drop the "prime" for the equations in the rotating grid hereafter.

3.1. Stroboscopic matching

We look for a solution of the above Eqs. (4) and (5) by expanding the fields Φ and $\bar{n}$ in spherical harmonics

$$\Phi = \sum_{\ell m} P_\ell^m(\cos\theta)\left[a_{\ell m}\cos(m\varphi) + b_{\ell m}\sin(m\varphi)\right], \tag{7}$$

$$\bar{n} = \sum_{\ell m} P_\ell^m(\cos\theta)\left[\bar{n}^c_{\ell m}\cos(m\varphi) + \bar{n}^s_{\ell m}\sin(m\varphi)\right]. \tag{8}$$

where the coefficients $a_{\ell m}(\xi,\tau)$ and $b_{\ell m}(\xi,\tau)$ are the unknown functions, and $P_\ell^m(\theta)$ are the Legendre associate functions. Similarly, $\bar{n}^c_{\ell m}$ and $\bar{n}^s_{\ell m}$ are the components of the source $\bar{n}$. In the inner domain ($\xi \leq 1$), we obtain a system of two coupled partial differential equations for each value of ℓ and m (recall that we now use $\tau = \tau'$):

$$\begin{aligned} &\left[\frac{\partial^2}{\partial\tau^2} - C^2\left(\frac{\partial^2}{\partial\xi^2} + \frac{2}{\xi}\frac{\partial}{\partial\xi} - \frac{\ell(\ell+1)}{\xi^2}\right)\right. \\ &\left. - (2\pi)^2m^2\right]a^<_{\ell m} + 2(2\pi)m\frac{\partial}{\partial\tau}b^<_{\ell m} = \bar{n}^c_{\ell m}, \end{aligned} \tag{9}$$

where N denotes the number of degrees of freedom in a given dimension. As it has been said, in the present case the number of operations is proportional to $N_\theta \cdot N_\varphi$.

and

$$\left[\frac{\partial^2}{\partial\tau^2} - C^2\left(\frac{\partial^2}{\partial\xi^2} + \frac{2}{\xi}\frac{\partial}{\partial\xi} - \frac{\ell(\ell+1)}{\xi^2}\right) - (2\pi)^2 m^2\right] b^<_{\ell m} - 2(2\pi)m\frac{\partial}{\partial\tau}\, a^<_{\ell m} = \bar{n}^s_{\ell m}. \tag{10}$$

Similarly, for the external domain ($\xi \geq 1$) we find:

$$\left[\frac{\partial^2}{\partial\tau^2} - C^2\left(\frac{\partial^2}{\partial\xi^2} + \frac{2}{\xi}\frac{\partial}{\partial\xi} - \frac{\ell(\ell+1)}{\xi^2}\right)\right] a^>_{\ell m} = 0 \tag{11}$$

$$\left[\frac{\partial^2}{\partial\tau^2} - C^2\left(\frac{\partial^2}{\partial\xi^2} + \frac{2}{\xi}\frac{\partial}{\partial\xi} - \frac{\ell(\ell+1)}{\xi^2}\right)\right] b^>_{\ell m} = 0. \tag{12}$$

By taking into account the expression of the "light velocity" given by Eq. (6) and the inequality $m \leq \ell$, we can see that the second-order differential spatial operator appearing in Eqs. (9), (10) is of definite type if $R_L \geq R_*$.

In order to solve these equations we make use of a multi-domain spectral technique in the radial direction and finite differences in the time variable. In our specific implementation, for each couple of values (ℓ, m) and in each domain we construct a particular solution as well as the relevant homogeneous solutions; in our simple case, regularity of the solution at the origin leaves a single homogeneous solution in the interior domain [14], whereas in the exterior domain there are two homogeneous solutions. Solutions to Eqs. (9)-(10) in the inner domain and to (11)-(12) in the outer domain are written as linear combinations of the calculated homogeneous and particular solutions, thus involving in total three coefficients to be fixed. The latter are determined by: *i*) imposing an outgoing Sommerfeld wave condition on $\Phi^>$ at the outer boundary of the exterior domain (see e.g. Ref. [27]),

$$\left[\left(\frac{\partial}{\partial\tau} + \frac{\partial}{\partial\xi} + \frac{1}{\xi}\right)\Phi^>\right]_{\xi=\xi_D} = 0, \tag{13}$$

where ξ_D is the external radius of the outer domain; *ii*) enforcing the continuity of the fields $\Phi^<$ and $\Phi^>$, and *iii*) of their radial derivatives $\Phi'^<$ and $\Phi'^>$, at the intermediate boundary $\xi = 1$. This makes three conditions for three homogeneous solutions and the matching system is invertible.

The following discussions focus on the two last points, i.e. the matching conditions at $\xi = 1$, for a given value of the angle θ_i, $i \in \{1, ..., N_\theta\}$. In our scheme we employ the same number of sampling points in the φ direction, N_φ, in the two grids. Using an index $j \in \{1, ..., N_\varphi\}$, let us denote by $\Phi^<_j(\tau)$ and $\Phi'^<_j(\tau)$ the values of the field $\Phi^<(\tau, \xi = 1, \theta = \theta_i, \varphi = \varphi_j)$ and its radial derivative $\Phi'^<(\tau, \xi = 1, \theta = \theta_i, \varphi = \varphi_j)$ on the φ-sampling points in the inner grid, and by $\Phi^>_j(\tau)$ and $\Phi'^>_j(\tau)$ the analogous values of $\Phi^>(\tau, \xi = 1, \theta = \theta_i, \varphi = \varphi_j)$ and $\Phi'^>(\tau, \xi = 1, \theta = \theta_i, \varphi = \varphi_j)$ in the outer domain.

Then, at the initial time $\tau = \tau_o$, we choose the sampling points of the two grids to coincide. In this situation we use strong matching techniques*, that are simply expressed as:

$$\begin{array}{ccc} \Phi^<_1(\tau_0) = \Phi^>_1(\tau_0) & , & \Phi'^<_1(\tau_0) = \Phi'^>_1(\tau_0) \\ \Phi^<_2(\tau_0) = \Phi^>_2(\tau_0) & , & \Phi'^<_2(\tau_0) = \Phi'^>_2(\tau_0) \\ & \cdots & \\ \Phi^<_{N_\varphi}(\tau_0) = \Phi^>_{N_\varphi}(\tau_0) & , & \Phi'^<_{N_\varphi}(\tau_0) = \Phi'^>_{N_\varphi}(\tau_0) \end{array} \tag{14}$$

* Alternatively, variational (weak) matching methods could be used. Penalty terms can also be introduced if this is suggested by the complexity of the system.

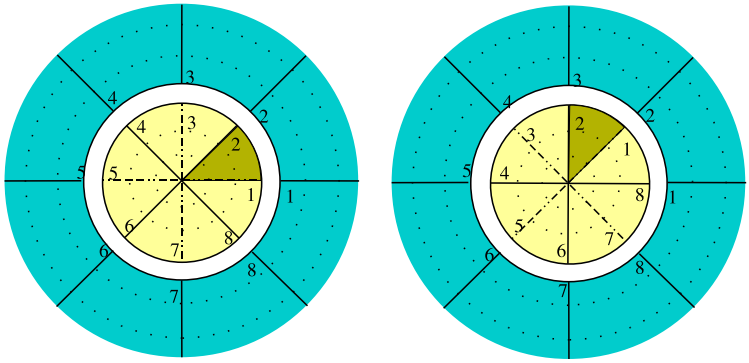

Figure 1. Choice of evolution step $\delta\tau$, adjusted to the sampling interval $\delta\varphi$, so as to guarantee the (*stroboscopic*) coincidence of the $\varphi-$sampling points corresponding to the interior and the exterior grids along the whole time evolution.

This makes $2N_\varphi$ conditions for each value θ_i, which is the right number of matching relations. Regarding the choice of the evolution time step $\delta\tau$, two situations may occur: if one uses an explicit time-evolution scheme, it must satisfy the stability Courant conditions; on the other hand, if the time-integration scheme is implicit (more precisely, A-stable), then the time-step is not limited. Let us first suppose that this is the case and let us choose $\delta\tau = \frac{\delta\varphi}{2\pi}$, where $\delta\varphi = \frac{2\pi}{N_\varphi}$ is the sampling $\varphi-$angular interval. With this choice of $\delta\tau$ the sampling points at $\tau = \tau_{\rm o} + k\cdot\delta\tau$, with $k \in \{0, 1, 2, ...\}$, do coincide again at any later time (see Fig. 1). The matching for a step k is simply given by:

$$\begin{array}{ccc} \Phi^{<}_{1} = \Phi^{>}_{(1+k)\mathrm{mod}(N_\varphi)} & , & \Phi'^{<}_{1} = \Phi'^{>}_{(1+k)\mathrm{mod}(N_\varphi)} \\ \Phi^{<}_{2} = \Phi^{>}_{(2+k)\mathrm{mod}(N_\varphi)} & , & \Phi'^{<}_{2} = \Phi'^{>}_{(2+k)\mathrm{mod}(N_\varphi)} \\ & \cdots & \\ \Phi^{<}_{N_\varphi} = \Phi^{>}_{(N_\varphi+k)\mathrm{mod}(N_\varphi)} & , & \Phi'^{<}_{N_\varphi} = \Phi'^{>}_{(N_\varphi+k)\mathrm{mod}(N_\varphi)}. \end{array} \tag{15}$$

We now consider the more general case in which $\delta\tau$ is bound to be smaller than a given critical value, given for instance by the Courant condition. Our strategy consists in choosing a $\delta\tau$, satisfying $\delta\tau = \frac{1}{2\pi\cdot K}\delta\varphi$ where K is a sufficiently large integer number. In this case, the sampling points only coincide after K time steps, and therefore we need to interpolate at supplementary points in the φ coordinate (see Figure 2). At this stage, spectral techniques provide an straightforward manner to proceed by performing an "oversampling" of the spectral description. That is, given the original N_φ coefficients codifying the behavior of the function in the φ direction and corresponding to the N_φ sampling points [e.g. $(a_{\ell 1}, a_{\ell 2}, ..., a_{\ell N_\varphi})$ for a given ℓ], one increases the number of sampling points in φ by a factor K, in such a manner that the new coefficients, counterpart of the new points, are set to zero: the information is encoded in the same number of non-vanishing coefficients but in a space with a bigger number of degrees of freedom:

$$(a_{\ell 1}, a_{\ell 2}, ..., a_{\ell N_\varphi}, \underbrace{\overbrace{0, ..., 0}^{N_\varphi \text{ times}}, ..., 0, ..., 0}_{(K-1)\cdot N_\varphi \text{ times}}). \tag{16}$$

The values at the new (interpolation) points can be obtained by performing the inverse Fourier transform on the larger set of coefficients. Moreover, a Fast Fourier

Transform algorithm could be used only involving a number of operations proportional to $(N_\varphi \cdot K)\log(N_\varphi \cdot K)$ for each ℓ. Once the matching is done, in an analogous manner to the one described in conditions (15), only N_φ coefficients are kept in order to codify the function Φ at each domain. Proceeding in this way, the functions $\Phi^<$, $\Phi'^<$ and $\Phi^>$, $\Phi'^>$ can be interpolated at the Gauss-Radau sampling points of the Fourier expansion. These Gauss-Radau sampling points are "smart" sampling points for which the following identity holds

$$\int_0^{2\pi} \cos(k\phi)\cos(m\phi)d\phi = \sum_{j=0}^{N-1} \cos(2\pi kj/N_\varphi)\cos(2\pi mj/N_\varphi)$$

$k,\ m,\ j$ being integer positive numbers and $k,\ m \leq N_\varphi/2$ (analogous relations for other trigonometric functions). If the solution of the above system of equations does not contain spatial frequencies (in the Fourier expansion) larger than $N_\varphi/2$, then a solution obtained with a number of degrees of freedom higher than N_φ will give the same result (within round-off errors); therefore the interpolation is exact.

Even though the previous discussion illustrates the underlying philosophy, the method presented above is not the most efficient one. As a matter of fact, there is a manner to by-pass the inverse Fourier transform step, gaining a factor $\log N$ in each angular direction. This is accomplished by making the matching in the coefficient space rather than in the configuration values of the functions Φ. For this, we must expand the inner and outer solutions in the same φ-coordinate expansion bases. This can be achieved straightforwardly, since the respective bases [$\cos(m\varphi')$ and $\sin(m\varphi')$ in the inner domain, and $\cos(m\varphi)$ and $\sin(m\varphi)$ in the outer domain], are related by a simple rotation: $\delta\varphi = \varphi' - \varphi = \Omega\delta t = 2\pi\delta\tau$. Therefore, given the function $F(\varphi') = \Phi^<(\tau, \xi = 1, \theta, \varphi')$ in the inner domain with

$$F(\varphi') = \sum_{m=0}^{N_\varphi - 1} \left(a'_m \cos(m\varphi') + b'_m \sin(m\varphi')\right), \tag{17}$$

the standard trigonometric relations provide the coefficients a_m and b_m in the φ bases employed in the outer domain, and necessary for performing the matching:

$$\begin{aligned} a_m &= a'_m \cos(m\,\delta\varphi) + b'_m \sin(m\,\delta\varphi) \\ b_m &= -\,a'_m \sin(m\,\delta\varphi) + b'_m \cos(m\,\delta\varphi) \end{aligned} \tag{18}$$

If $\delta\varphi = 2\pi/N_\varphi$, this is equivalent to sample the function $F(\varphi)$ at the Gauss-Radau points and to come back in the Fourier space. In other words, the matching is done without leaving the Fourier space, but at the cost of (again) oversampling points in the φ-direction by a factor K. The number of operation is proportional to $N_\theta \cdot N_\varphi$. A bonus of this strategy, that we refer to as *stroboscopic*, is the following: the technique described above prevents the appearance of spurious time frequency terms generated by the beating between the rotation frequency and the time sampling frequency. This terms could spoil the study of the numerically constructed signal, in e.g. an a posteriori time Fourier transform analysis of the emitted radiation.

3.2. Implementation

Equations (9)-(10) and (11)-(12) are solved by using the spectral methods developed in our group [28].

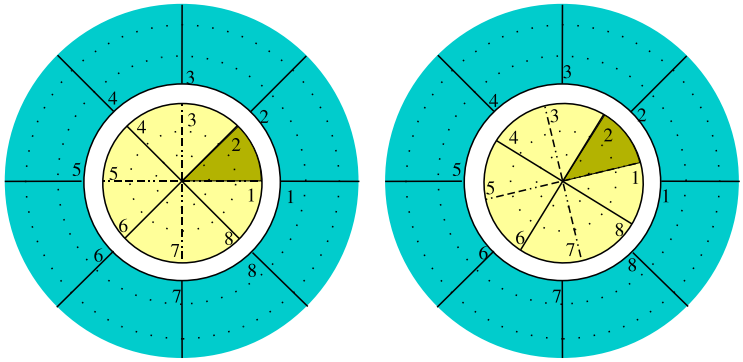

Figure 2. Choice of evolution step $\delta\tau$ as an integer fraction (in this case $K = 3$) of the $\varphi-$sampling interval $\delta\varphi$. In this case, interpolation of the points is needed for enforcing the matching. This is achieved in a *fast* manner by employing a spectral oversampling technique based on the Gauss-Radau points.

For the time evolution in the non-rotating domain [i.e. Eqs. (11) and (12)] we use a second-order implicit Crank-Nicolson scheme. In addition, Sommerfeld outgoing boundary conditions are imposed at the outer boundary.

Regarding the rotating domain, which contains the coordinate singularity at $\xi = 0$, we perform an expansion on a Galerkin basis satisfying the regularity conditions [14]. Moreover, the wave operator is also treated implicitly with a second-order Crank-Nicolson scheme and the coupling terms containing first-order time derivatives are treated explicitly by making a second-order extrapolation from known values at previous time steps. An implicit treatment of those terms could be more appropriate but not necessary.

4. Tests

We perform two tests of the scheme previously described.

4.1. Comparison with an analytical solution

The first example deals with the comparison between the numerical and the analytical solutions, in the restricted case of a helically symmetric operator obtained from Eq. (9) or Eq. (10) by setting to zero the time derivatives. The resulting differential operator, L, has the following form

$$L = \frac{d^2}{d\xi^2} + \frac{2}{\xi}\frac{d}{d\xi} - \frac{\ell(\ell+1)}{\xi^2} + \left(\frac{2m}{\pi}\right)^2. \tag{19}$$

A straightforward manner to proceed consists in obtaining the source n by the application of the operator L to a potential Φ given analytically. We choose the form of the potential Φ to be

$$\Phi(\xi) = \frac{\xi^4}{\sqrt{\xi}} J_{\ell+1/2}(\xi), \tag{20}$$

with $J_{\ell+1/2}$ being the semi-integer Bessel function of the first kind. In this case, the only modes in (19) correspond to $\ell = 2$ and $m = 2$. The source n computed in this way determines the right-hand-side in Eqs. (9) and (10). The numerical

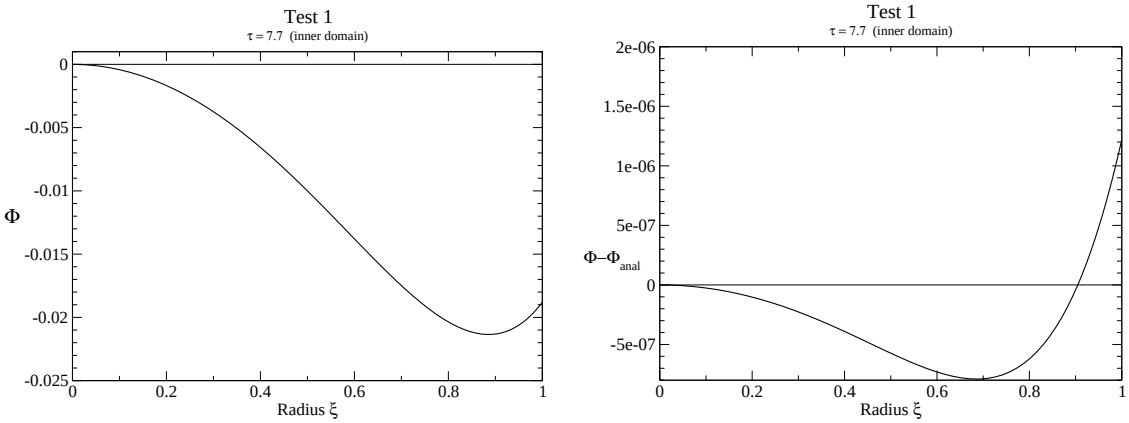

Figure 3. Comparison between the numerical and analytical solutions of Test 1. Left figure shows the solution at the end of the run ($\tau = 7.7$) and right figure the absolute difference between the numerical and the analytical solutions in the inner region.

solution obtained by the application of the present scheme is then compared to the corresponding analytical solution. The latter is expressed, in the inner domain, as a linear combination of the exact particular solution (20) and the regular homogeneous solution of the operator (19), which can be expressed in terms of the semi-integer Bessel function of the first kind $\eta(\xi) = \frac{1}{\sqrt{\xi}} J_{\ell+1/2}(\xi)$, that can be easily evaluated because it reduces to the sum of $\ell+1$ terms. Regarding the homogenous solution in the external domain, this is expressed in terms of a second order Bessel function $H_{\ell+1/2}(\xi)$. Once the matching conditions at R_* and the Sommerfeld boundary conditions at ξ_D are imposed, the explicit comparison with the analytical solution can be done, finding a very good agreement (cf. Figure 3 for a quantitative assessment).

The tests above concern the case $\ell = 2$ and $m = 2$, when a helical symmetry is present in the source. The number of points used are $N_\varphi = N_\theta = 4$, $N_r^{\rm inner} = 65$ in the inner domain (for $\xi \in [0,1]$), $N_r^{\rm outer} = 257$ in the outer domain (for $\xi \in [1,21]$), and a time step $\delta\tau = (1024)^{-1}$. This case $\ell = 2$ and $m = 2$ has been chosen because it is relevant for gravitational wave emission in General Relativity. The choice of a symmetry in the source simplifies the comparison between analytical and numerical results.

We have studied the convergence behavior of the code with the same settings, but changing the number of radial coefficients in both domains, while keeping fixed the ratio $N_r^{\rm outer}/N_r^{\rm inner} = 8$. In particular, we have checked that the difference between the numerical and analytical solutions would decay as e^{-N_r}, which is the expected rate for spectral approximation series of smooth functions. This check is displayed in Figure 4, where the discrepancy saturates at about 10^{-6} level, due to numerical limitations. There are two sources accounting for this accuracy level, whose behaviors were clearly identified in numerical investigations: first, the time finite-differencing errors, which are linked to the second-order time-scheme, and then the use of approximate boundary conditions (we remind that Sommerfeld boundary conditions are exact only for $\ell = 0$ modes) at $\xi = \xi_D$. We have checked that these latter errors would decay as ξ_D^{-2}, which is the predicted rate (see also [27]).

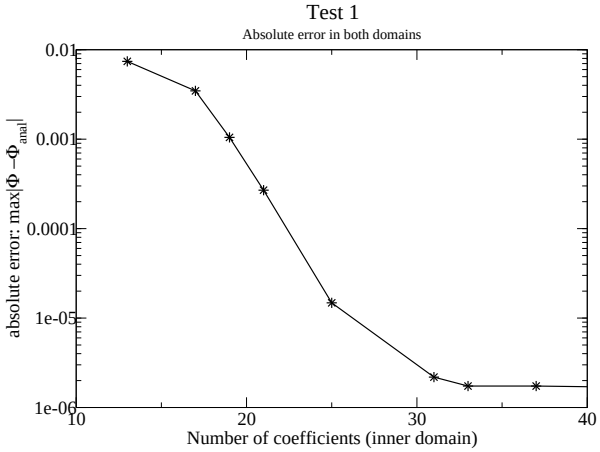

Figure 4. Behavior of the accuracy obtained in Test 1 (see also Figure 3) as a function of the number of radial spectral coefficients. The displayed numbers correspond to the inner domain; in the outer domain eight times more coefficients have been used.

4.2. Conservation of helical symmetry

The second test to our resolution scheme studies how a solution Φ to Eqs. (1) and (2) "tracks" a symmetry present in the prescribed matter source. More specifically, we consider a source n which is rigidly rotating with respect to the inertial frame with an angular velocity Ω. We choose its form as

$$n = n_0 \left[\left(\frac{r}{R_*} \right)^4 - \left(\frac{r}{R_*} \right)^2 \right] \sin^2\theta \cos(2\varphi + 2\Omega t). \tag{21}$$

This source is symmetric with respect to the helical vector $\zeta \equiv \partial_t - \Omega \partial\varphi$, i.e.

$$\left(\frac{\partial}{\partial t} - \Omega \frac{\partial}{\partial \varphi} \right) n = 0. \tag{22}$$

Because of the existence of this symmetry, we expect the solution Φ to present also the helical symmetry once a sufficient time has been elapsed (once it has reached some "stationary" regime).

We apply to this simple case the scheme described in section 3. Regarding the inner rotating domain, since the only non-vanishing terms correspond to $\ell = 2$ and $m = 2$, Eqs. (9) and (10) read as follows:

$$\begin{aligned} &\frac{\partial^2 a^<}{\partial \tau^2} + (2\pi) \left(4 \frac{\partial b^<}{\partial \tau} - (2\pi) 4 a^< \right) \\ &- C^2 \left(\frac{\partial^2}{\partial \xi^2} + \frac{2}{\xi} \frac{\partial}{\partial \xi} - \frac{6}{\xi^2} \right) a^< = \bar{n}(\xi) \end{aligned} \tag{23}$$

$$\begin{aligned} &\frac{\partial^2}{\partial \tau^2} b^< - (2\pi) \left(4 \frac{\partial a^<}{\partial \tau} + 4(2\pi) b^< \right) \\ &- C^2 \left(\frac{\partial^2}{\partial_\xi^2} + \frac{2}{\xi} \frac{\partial}{\partial \xi} - \frac{6}{\xi^2} \right) b^< = 0 \end{aligned} \tag{24}$$

where for shortness, we have written respectively $a^< = a^<_{22}$, $b^< = b^<_{22}$ and $\bar{n} = R_*^2 \cdot C^2 n_{22}$. Note that in the inner rotating frame, the source $\bar{n}$ does not depends on τ and $\bar{n}^s = 0$. In the exterior non-rotating domain we solve the similar expressions coming from Eqs. (11) and (12).

Initial conditions are chosen such that $a = b = 0$ at $\tau = \tau_0$, and the evolution is induced by the source $\bar{n}$ (see Fig. 6a, where the profile at the first time-step is given). This was computed in a such way to ensure the continuity of the solution and its derivative across the boundary $r = R_*$. The dynamical evolution began at time $\tau = \tau_o = 0$, and the numerical settings were slightly different from those of the first tests, namely: $N_r^{\rm inner} = 33, N_r^{\rm outer} = 129, N_\theta = 4, N_\varphi = 4$ and $\delta\tau = (512)^{-1}$.

We study the emergence of the helical symmetry in the evolving dynamical solution in two different manners:
i) First we assess the verification of the symmetry conditions given by the Eq. (22), for the case of the constructed numerical solution. This provides a good self-consistent test of the accuracy of the solution. In the present case, we compute the quantity δa, defined as

$$\delta a := \frac{\partial a}{\partial \tau} - \Omega \frac{\partial a}{\partial \varphi} \tag{25}$$

where a is considered as a function of ξ and τ, and we study its evolution in time. Figure 5.a shows the evaluation of (25) on the numerical solution: after the transient due to the switch on of the evolution, the solution must asymptotically verify $\delta a = 0$. Relative error, computed at $\xi = 1$ in the outer region, is plotted versus the time τ. Figure 5.b shows the difference between the computed solution and the solution of the Poisson equation for Φ (instead of the wave equation (1), to show propagation effects). The actual solution differs qualitatively with respect to the non-propagating one by a phase-$(\pi/2)$ quadrature term that is showed in Figure 5.c. This term is responsible of the radiation reaction force (or braking force), and we have checked that this term scales as $(R_*/r)^5$ as predicted by the analytical properties for an $\ell = 2$ propagation mode. Note that the solution of the Poisson equation, i.e. satisfying the equation $\bar{\Delta} a^< = -\bar{n}$, is

$$a^<(\xi, 0) = n_0 \left(\frac{\xi^4}{14} - \frac{\xi^6}{36} + \alpha \xi^2 \right), \quad a^>(\xi, 0) = \frac{n_0 \beta}{\xi^3}, \tag{26}$$

where $\alpha = (1/20 - 1/14)$ and $\beta = (1/45 - 1/35)$.

Finally, Figure 6 presents some radial profiles at various moments of the numerical solution to Eqs. (23) and (24).
ii) A second way to proceed in order to study the emergence of the helical symmetry in the solution, consists in comparing the previous dynamical solution with the one corresponding to a system obtained by neglecting the time derivative terms in Eqs. (9)-(10), in the inner domain. In this case the problem in the rotating region becomes an elliptic one, and it can be solved easily by inverting the operator L given in Eq. (19), whereas we still solve for the wave operator in the outer domain. Note that it is crucial for the ellipticity of this operator L the fact that the rotating grid is set inside the light cylinder. If this were not be the case, we would have a mixed-type differential operator (see e.g. [26]). Given the second-order Crank-Nicolson scheme we have employed, results computed with the method *i*) and the method *ii*) differ only by quantities of second order in $(\delta\tau)^2$. As a complementary test to the emergence of the helical symmetry, Figure 7 shows evaluation of (25) on the numerical solution to the symmetry-reduced operator (19). Note that the solution reaches the stationary regime

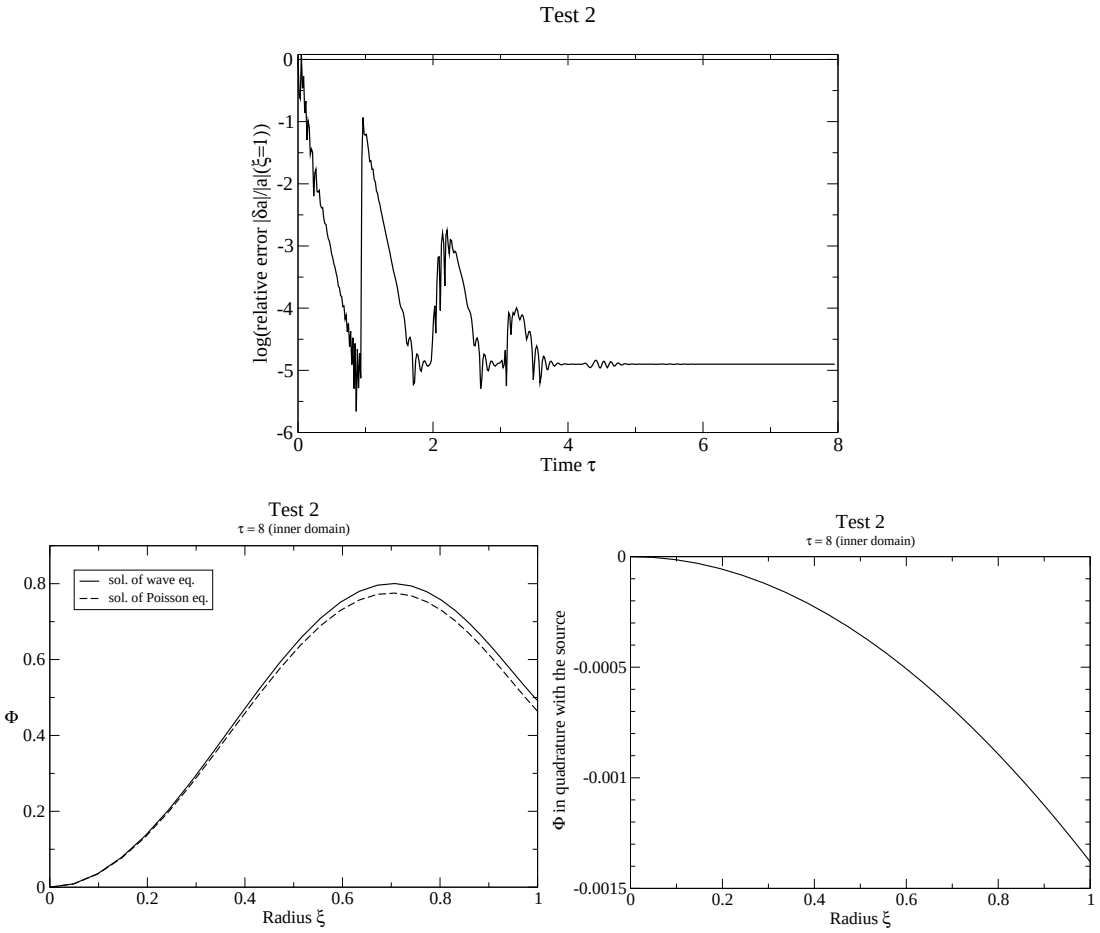

Figure 5. Fig. 5a: Relative error δa for Test 2 in a logarithmic scale versus the time τ, for $R_L/R_* = 3$. The huge spike at time $\tau = 1$ is due to terms containing first time derivatives in Eqs. (9), (10) that are switched on only at $\tau = 1$ in order to avoid a strong oscillation at the beginning of the simulation. The plateau reached by the error is due to time-differentiation and scales like $\delta\tau^2$. Fig. 5b: The actual solution of the wave equation in the rotating region (upper curve) and the solution of the Poisson equation. Fig. 5c: Component of the solution Φ in quadrature with the source.

much faster than when solving the full wave equation. The big bump appearing at the time $\tau \sim 3.2$ and the small one at the time $\tau \sim 5.5$ are generated by a partial reflexion at the external boundary of the external domain due to the approximate outgoing Sommerfeld boundary conditions [which are exact for $\ell = 0$; see Eq. (13)]. We have checked that the amplitude of the bumps scales as the inverse of the square of the dimension of the external grid, as predicted by the theory.

5. Discussion and conclusions

The rationale of this work is the following: a class of physical problems (rotating stars or orbiting stars/black holes) are easily treated in corotating grids. However,

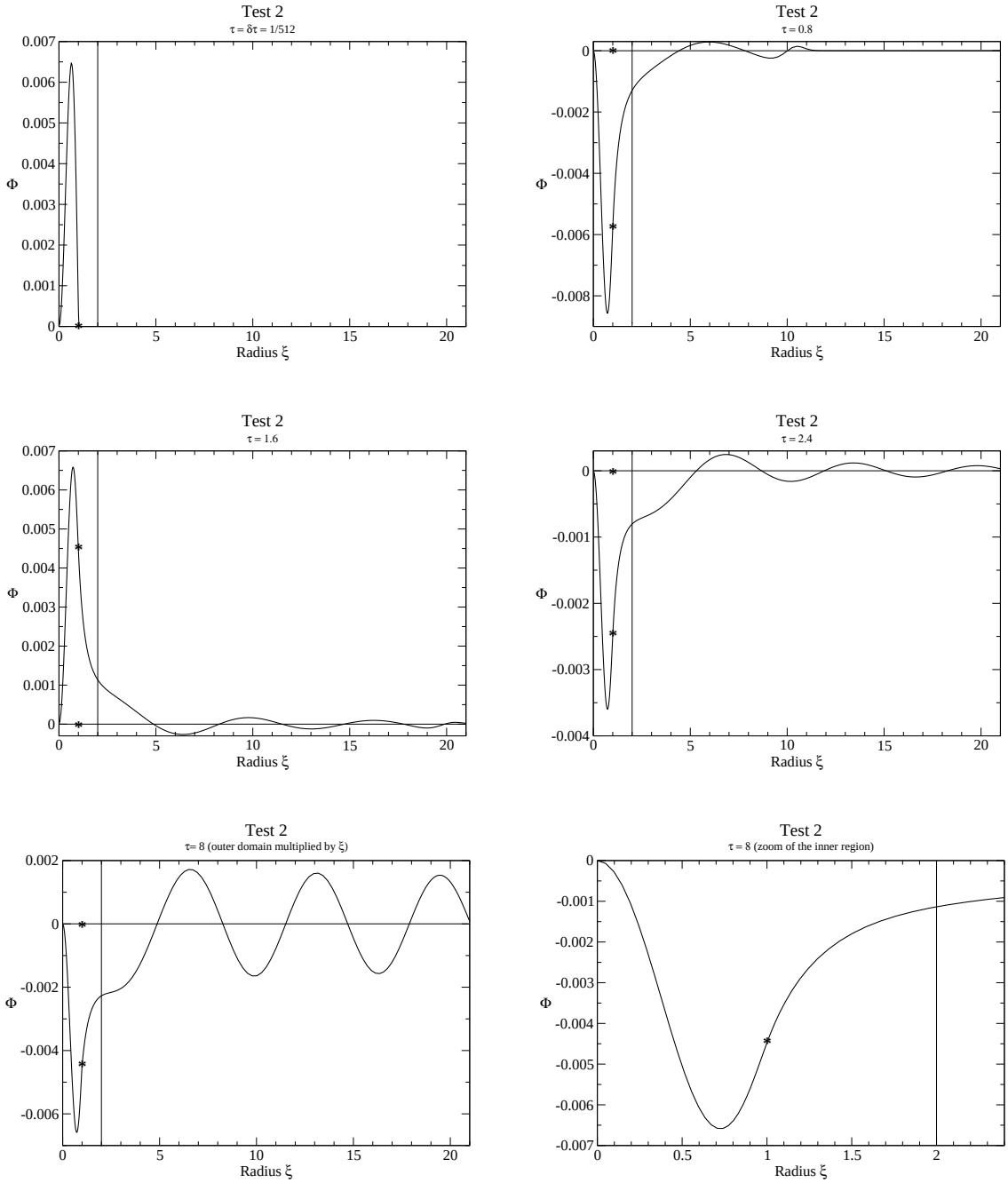

Figure 6. Figures 6.a-e show some snapshots of the solution in Test 2, with $R_L/R_* = 2$ at different times. At $\xi = 1$ the "star" shows the frontier between the rotating and inertial domains. The vertical line at $\xi = 2$ indicates the light cylinder. On Fig. 6.e the solution in the external region was multiplied by ξ in order to better visualize the solution at the edge of the external grid. Figure 6.f is a zoom of the solution inside and near the light cylinder. The dimensionless "light velocity" is $C = 4\pi$.

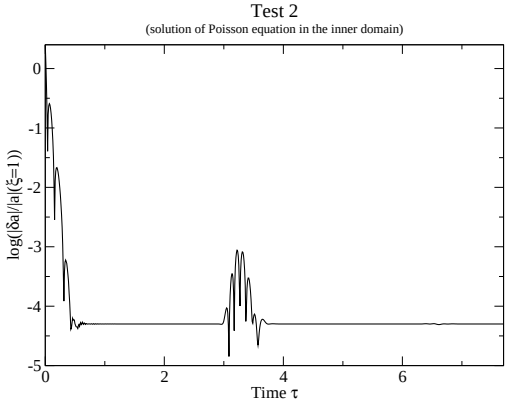

Figure 7. Test of the helical symmetry δa as in Fig. 5a.

analytical and numerical problems show up associated with the existence of a light cylinder. We have described a technique to match the solution computed in an inner rotating domain of external radius R_*, with the solution in an outer non-rotating domain under the condition $R_* < R_L$, where $R_L = c/\,\Omega$ is the light cylinder radius. The matching technique is independent of the manner of obtaining the solutions in each domain. In typical physical situations, the restriction $R_* < R_L$ on the radius is not severe: for example in the worst case for orbiting neutron stars, we have $\Omega \sim 4000\ s^{-1}$ [29] and $R_* \sim 20$ km, providing a ratio $R_L/R_* \sim 4$. As a more extreme case, this ratio for orbiting black holes before the merger is not smaller than 2. A typical problem to be treated with the technique described here, is the case two orbiting NS, for which the parameters of the orbit are known, and for which we want study small amplitude motions inside each star (convection r-modes and/or elliptical cylinder instabilities). The numerical study of these phenomena is easier in a domain in which the surface of the star does not move and boundary condition can be exactly imposed, as compared with a star traveling through the grid.

Regarding the numerical implementation, this is not the only scheme making use of multi-domain spectral methods in order to deal with the resolution of partial differential equations in rotating domains (cf. [10] in the general dynamical case and [25] in the helically symmetric situation). The specificity of our approach is the use of a rotating domain (our inner domain) that, unlike the case in other schemes, does not extend up to infinity. In particular our inner rotating domain does not go beyond the light cylinder, thus providing a simple treatment of this analytical and numerical issue. The results we have obtained are accurate, and quantities like the back-reaction force are correctly computed. We conclude that our "stroboscopic" matching technique is a simple and efficient tool for the description of relativistic rotating systems, and in particular for avoiding analytical and numerical problems linked with the existence of a light cylinder.

The technique described can be extended, *mutata mutandis*, to vectorial or tensorial equations, in particular choosing some convenient triad (or tetrad depending on the formulation), and projecting onto it the tensor components in order to deal with scalar quantities.

Finally, the case involving a non-constant angular velocity can also be treated: if the variation of the rotation period P in time is known, we can perform the coordinate transformation $t = t(\tau)$ generalizing Eqs. (3), in such a way that wave equations correcting Eqs. (4) and (5) with extra terms in $\frac{\partial t}{\partial \tau}$ are obtained. These additional terms are harmless for our scheme, provided that the ratio R_L/R_* is sufficiently large. All those possibilities are yet to be explored.

Acknowledgments

We thank Éric Gourgoulhon and Philippe Grandclément for helpful discussions. SB and JN were supported by the A.N.R. Grant 06-2-134423 entitled "Mathematical methods in general relativity" (MATH-GR). JLJ acknowledges the support of the Marie Curie European Reintegration contract MERG-CT-2006-043501 within the 6th European Community Framework Program, and the hospitality of the Observatoire de Paris.

References

[1] M. Alcubierre and B.F. Schutz, *Time symmetric ADI and causal reconnection*, in *Approaches to Numerical Relativity*, ed. R. d'Inverno (Southamptom), 1991.
[2] C. Bona, J. Massó and J. Stela, Phys. Rev. D **51**, 1639 (1995).
[3] F. Pretorius, Phys. Rev. Lett. **95**, 121101 (2005).
[4] U. Sperhake, B. Kelly, P. Laguna, K.L. Smith and E. Schnetter, Phys. Rev. D **71**, 124042 (2005).
[5] B. Szilagyi, D. Pollney, L. Rezzolla, J. Thornburg, J. Winicour, arXiv:gr-qc/0612150v2.
[6] M. Campanelli, C.O. Lousto, P. Marronetti and Y. Zlochower, Phys. Rev. Lett. **96**, 111101 (2006).
[7] J.G. Baker, J. Centrella, D. Choi, M. Koppitz and J. van Meter, Phys. Rev. Lett. **96**, 111102 (2006).
[8] B. Bruegmann, J.A. Gonzalez, M. Hannam, S. Husa, U. Sperhake and W. Tichy, arXiv:gr-qc/0610128v1.
[9] S. Bonazzola, E. Gourgoulhon, P. Grandclément, and J. Novak, Phys. Rev. D **70**, 104007 (2004).
[10] M.A. Scheel, H.P. Pfeiffer, L. Lindblom, L.E. Kidder, O. Rinne, and S.A. Teukolsky, Phys. Rev. D **74**, 104006 (2006)
[11] A. Ashtekar and B. Krishnan, Living Rev. Relativity **7**, 10 (2004) [Online article]: cited on 10 May 2007, `http://www.livingreviews.org/lrr-2004-10`; L. Andersson, M. Mars and W. Simon, Phys. Rev. Lett. **95** 111102 (2005); L. Andersson, M. Mars and W. Simon, arXiv:0704.2889v1 [gr-qc].
[12] E. Gourgoulhon, Astron. Astrophys. **252**, 651–663, (1991).
[13] S. Bonazzola, E. Gourgoulhon and J.-A. Marck, Phys. Rev. D **58**, 104020 (1998).
[14] S. Bonazzola, and J.-A. Marck, J. Comput. Phys. **87**, 201–230, (1990).
[15] S. Detweiler, Phys. Rev. D 50, 4929 (1994).
[16] S. Bonazzola, E. Gourgoulhon, and J.-A. Marck, Phys. Rev. D **56**, 7740 (1997).
[17] J.L. Friedman, K. Uryu, M. Shibata, Phys. Rev. D **65**, 064035 (2002).
[18] J.T. Whelan and J.D. Romano Phys. Rev. D **60**, 084009 (1999)
[19] J. T. Whelan, W. Krivan, and R. H. Price, Classical Quantum Gravity **17**, 4895 (2000)
[20] J. T. Whelan, C. Beetle, W. Landry, and R. H. Price, Classical Quantum Gravity **19**, 1285 (2002).
[21] R. H. Price, Classical Quantum Gravity **21**, S281 (2004).
[22] Z. Andrade et al., Phys. Rev. D **70**, 064001 (2004).
[23] B. Bromley, R. Owen and R.H. Price, Phys. Rev. D **71**, 104017 (2005)
[24] C. Beetle, B. Bromley, R.H. Price, Phys. Rev. D **74**, 024013 (2006).
[25] S.R. Lau, R.H. Price, Preprint: gr-qc/0702050.
[26] C. G. Torre, J. Math. Phys. **44**, 6223 (2003)
[27] J. Novak, S. Bonazzola, J. Comp. Phys. **197/1** 186-196 (2004).
[28] S. Bonazzola, E. Gourgoulhon, and J.-A. Marck, J. Comput. Appl. Math. **109**, 433–473, (1999).
[29] M. Bejger and al., A&A **431**, 297-306 (2005).